(Submitted for presentation at the Int'l Conf. on Accelerator Dosimetry and Experience to be held at the Stanford Linear Accelerator Center, Stanford, Calif., November 5-7, 1969.)

SLAC-PUB-686
(ACC)
Paper written: November 1969
Paper issued: July 1970

MEASUREMENT OF RADIAL AND LONGITUDINAL DOSE DISTRIBUTION IN A WATER PHANTOM IRRADIATED WITH A 10 GEV ELECTRON BEAM*

G. K. Svensson and W. R. Nelson

Health Physics Department
Stanford Linear Accelerator Center
Stanford University, Stanford, California 94305

ABSTRACT

The radial and longitudinal distribution of absorbed dose in a water phantom irradiated with 10 GeV electrons has been measured. The electron beam was well focussed, and the current was measured accurately with a toroid. Detector plates containing arrays of thermoluminescent ^{7}LiF dosimeters were inserted at different depths in the water tank. The profiles of the dose distribution were measured over six decades. The dose rate at different depths per unit incoming particle flux density will be presented and compared with two different Monte Carlo calculations by Alsmiller[2] and Beck.[3] The variation of the integral dose with electron energy is shown, and its possible significance discussed. The whole body dose versus peak dose for the delta-function type beam used in this experiment is shown.

Introduction

An experiment has been performed to determine the spatial distribution of the energy absorbed in a water tank irradiated by a 10 GeV electron beam. The measurement was done using thermoluminescent dosimeters (^{7}LiF) of various forms, located within a water tank having a total depth of 32.5 cm.

A similar experiment has been performed by Tesch[1] in order to study the longitudinal distribution of energy absorbtion in a 30 cm thick tissue equivalent medium.

Recent Monte Carlo calculations by Alsmiller[2] and Beck[3] give the energy deposited at a certain depth (z, Δz) in a semi-infinite water slab. The shape of the measured dose buildup in this experiment as well as absorbed dose to electron fluence conversion factors will be compared with their Monte Carlo calculations.

A discussion of the radiation hazard in the case of a person being accidentally hit by an electron beam will be presented and the concept of integral dose will be treated.

Equipment and Dosimetry

The lucite water tank was built of 1/2" thick lucite and the inner dimensions were 30 cm depth and 60 × 60 cm front area. The dosimeters were arranged in the detector arrays shown in Fig. 1. These are lucite plates with grooves and holes machined to hold LiF detectors. The inner square array holds 81 extruded rods† (1 mm diameter,

*Work supported by the U. S. Atomic Energy Commission.
†Harshaw Chemical Company, Cleveland, Ohio.

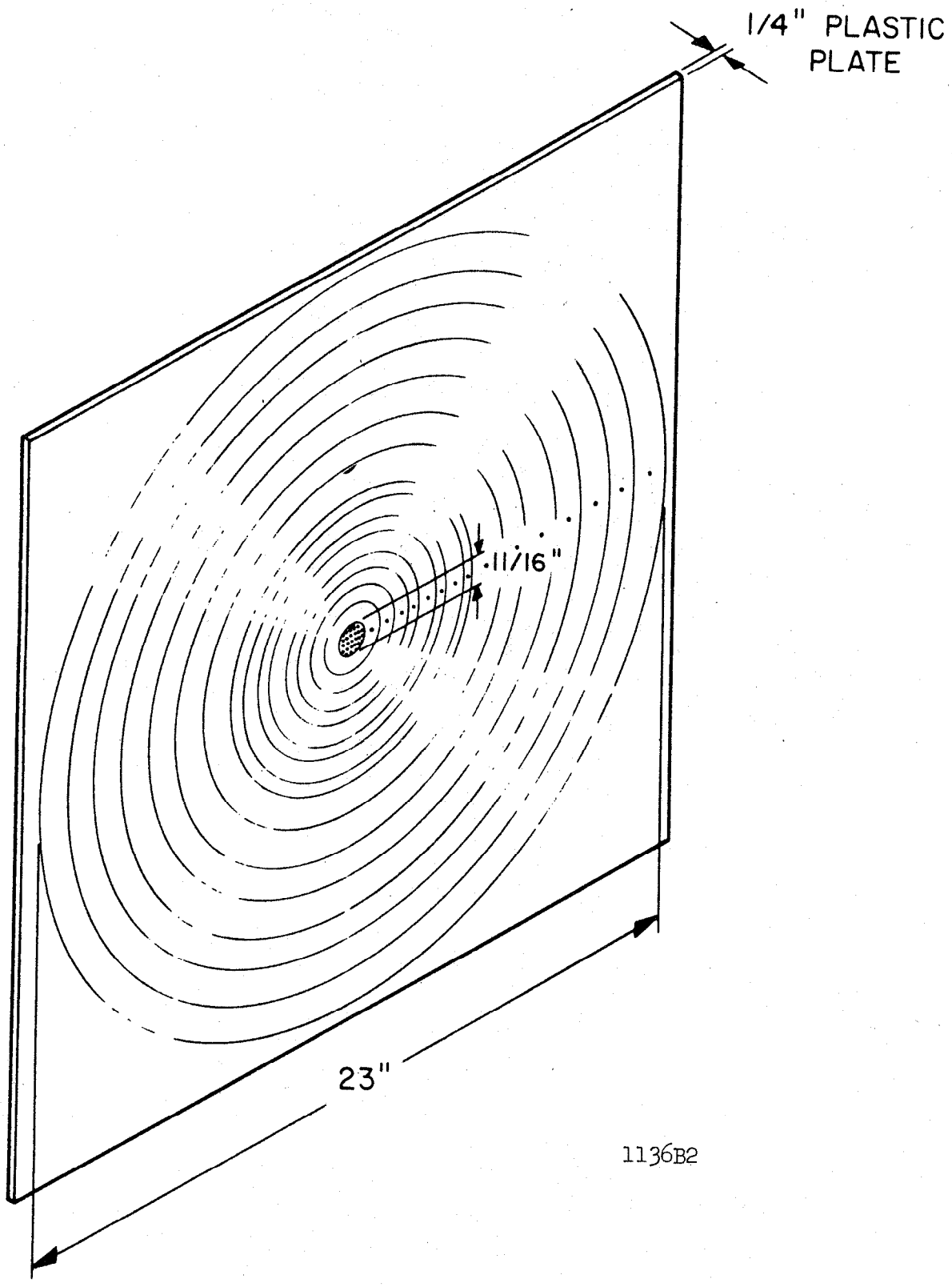

FIG. 1--Lucite plate used as detector holder for ^{7}LiF extruded rods (small holes) and ^{7}LiF powder in polyethylene tubing (rings). Array in center holds 81 rods.

6 mm long, $\rho = 2.6$ g/cm^{-3}) and the circles hold lengths of polyethylene tubing (0.965 mm OD and 0.584 mm ID) containing LiF powder which had a measured bulk density of 1.6 g/cm^{-3}. LiF will flow into such tubing easily if vibrated in. This detection system has been previously described.[4] Holes to hold extruded rods were also drilled between the grooves where strings were held.

Figure 2 shows the tank with the six detector plates in position. The first and last plates were quite close to the inner surfaces of the front and back wall of the tank respectively. To ensure that a well-focussed electron beam was centered on the center of the detector array, all the detector plates were aligned relative to each other within 0.25 mm. This was performed in a precision alignment laboratory. In spite of this the third plate was slightly misaligned due to a mishappening when the experimental procedure was executed. The data was subsequently corrected for this misalignment.

Calibration of the TLD was done on a ^{60}Co source installed in a concrete well. The source was collimated to reduce the scattered contribution from the concrete walls. From measurements of exposure (Victoreen condenser ion chambers), the absorbed dose in the medium in which the TLD was inserted was calculated.[5] In general, dosimeters of the size we use will perturb the flux of secondary particles in a medium; for example, 1.25 MeV photons from ^{60}Co will give rise to a mean initial Compton electron energy of 0.65 MeV. These have ranges of the order of 1 mm in pure LiF. The consequence is that the dosimeter response for this photon energy is the combined effect of the absorbed dose in the medium and in the dosimeter itself, and the absorbed dose that is calculated from an exposure-measurement is no longer the appropriate quantity, unless you have a matched wall-detector condition.[5]

Since we do have a fairly well-matched wall-detector condition in terms of atomic number and electron density, we have not applied any correction for this effect.

The fact that these dosimeters were used in a 10 GeV electron beam should not imply too many problems because 99% of the energy imparted from these incident electrons goes into the production of electrons (±) and photons (for the case of total shower absorbtion, at least). That is, the nuclear reactions are weak enough so that the so-called soft shower is not perturbed.[6] However, this argument does not prove that we can measure the absorbed dose with any high degree of accuracy (e.g., within a few percent) and one of our future tasks will be to perform an absolute calibration in a high energy electron beam.

Figure 3 shows the relative response as a function of absorbed dose for the extruded rods being used in this experiment. The supralinearity curve for ^{7}LiF powder was taken from R. C. Fix et al.[7]

Experimental Procedure

The experiment was performed in End Station A at the SLAC two-mile accelerator. The geometry is shown in Fig. 4. The following procedure was followed:

1. The electron beam was tuned up and steered to give a small beamspot on a ZnS screen. The energy of the beam was 10 GeV ± 0.5%.
2. Glass plates were exposed in order to determine the size and shape of the electron beam. The density of blackening of glass has been shown to be proportional to the electron fluence.[8]
3. A toroid charge monitor[9] located a few feet upstream of the experimental stand, was used to determine the electron current. To avoid overexposure of the ^{7}LiF the dose was not to exceed 10^5 rad. Based on the beam area (estimated from glass plate exposure) the number of electrons necessary to produce $< 10^5$ rad was calculated by using the appropriate mass stopping power value. The beam current and

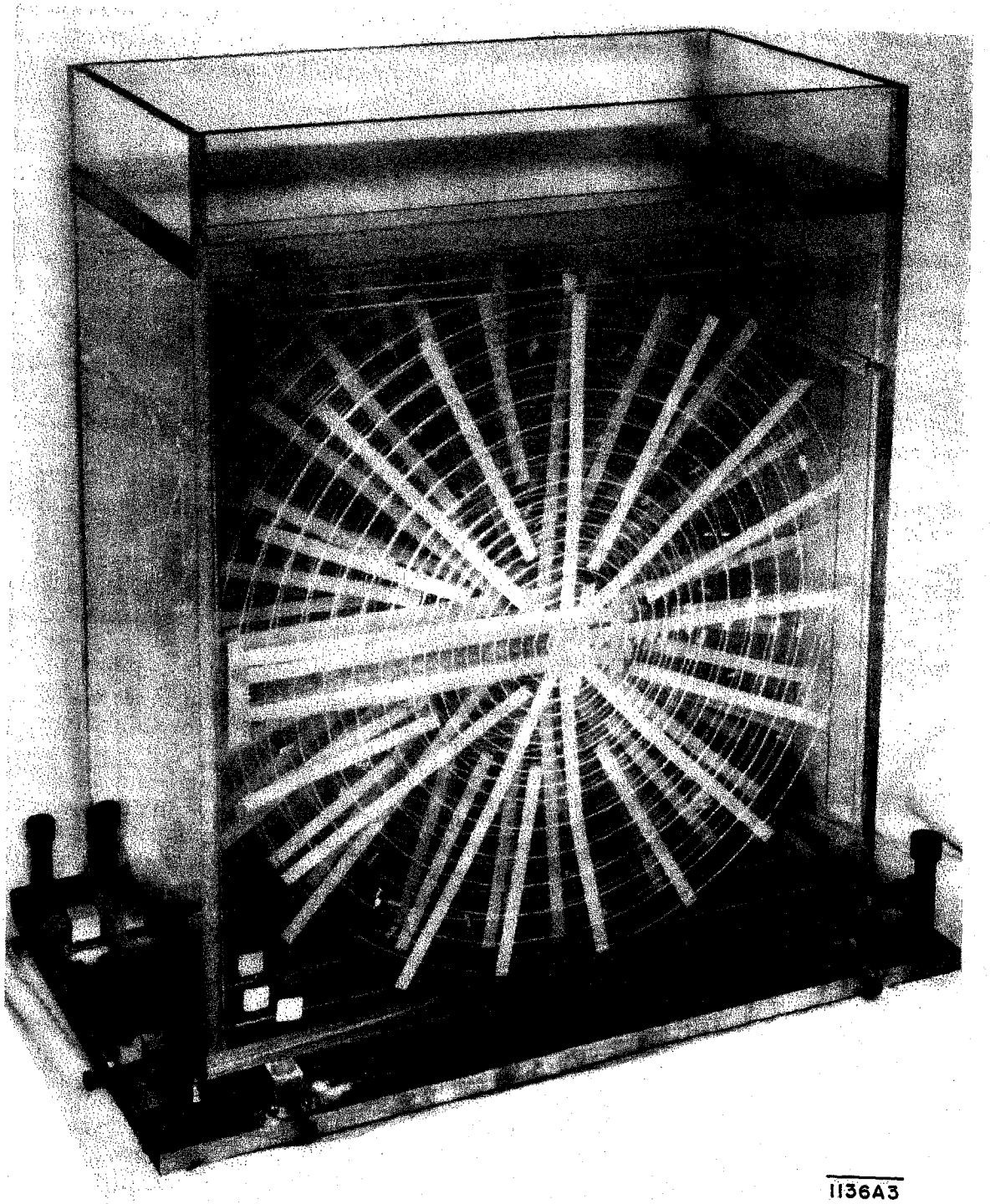

FIG. 2--Lucite water tank with the six detector plates in position.

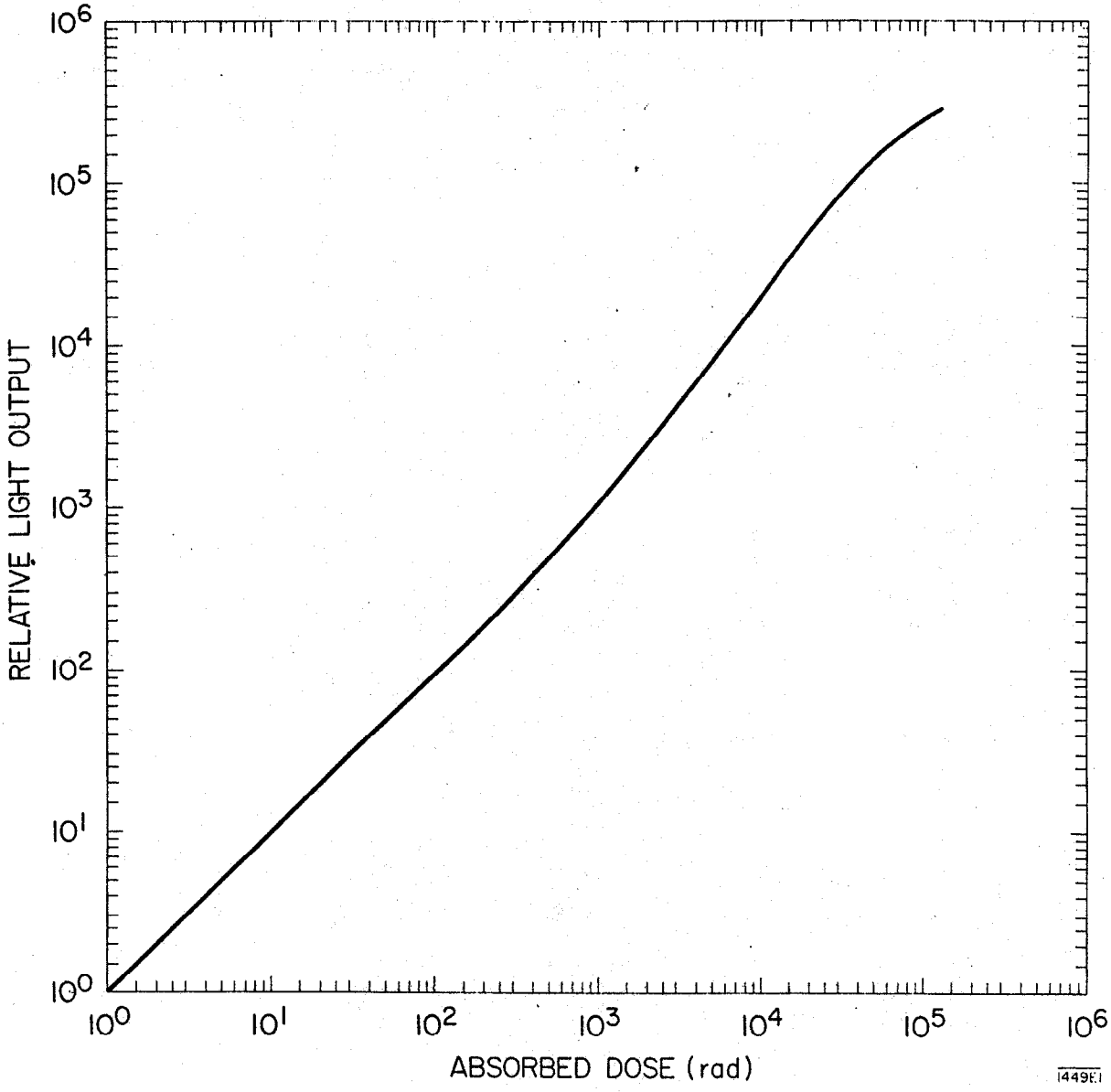

FIG. 3--Relative light output of ^{7}LiF extruded rods versus absorbed dose (rad) from ^{60}Co.

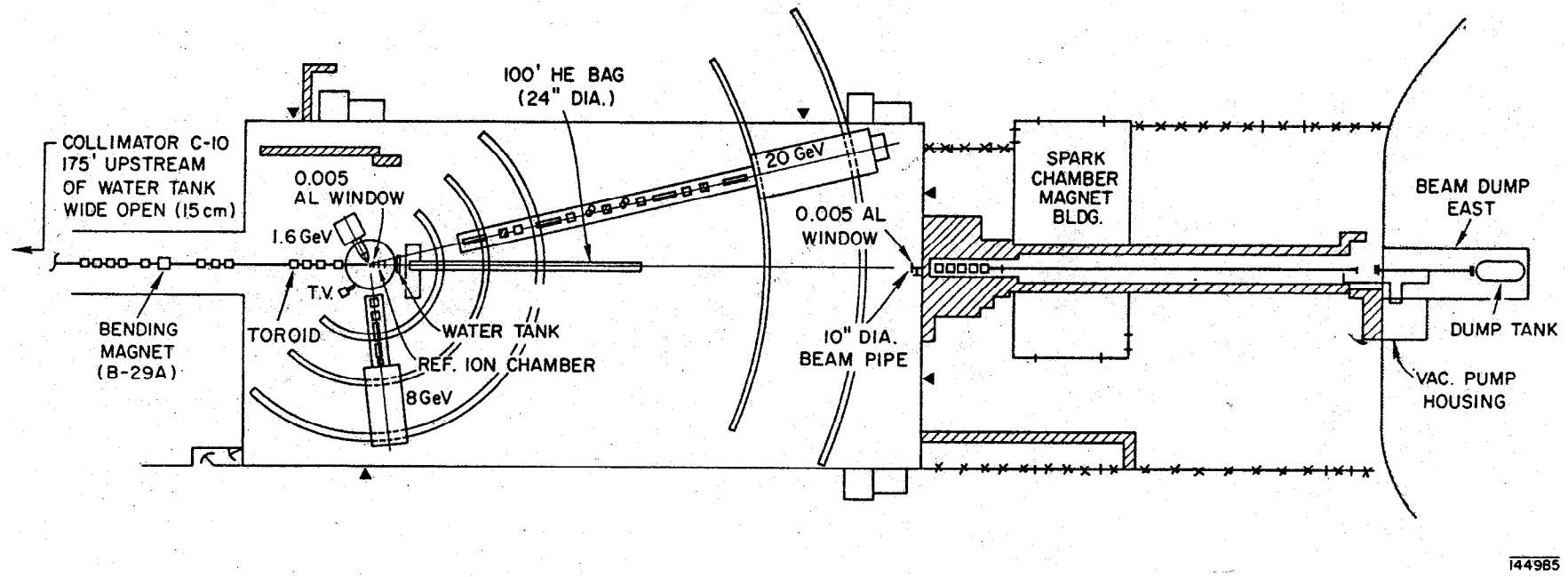

FIG. 4--Experimental arrangement of End Station A at SLAC, indicating the position of critical items; collimator C10, toroid, water tank and 100 ft. Helium bag.

exposure time was adjusted accordingly to give the correct number of electrons.

4. Two test exposures were performed to ensure that the TL dosimeters were indeed not overexposed when irradiated according to the above technique.

5. The six detector plates had already been aligned relative to each other as described earlier, and their location within the tank was established in such a manner that the plates could be removed and later re-positioned. With the detector plates removed, the tank itself was positioned on the experimental stand. The alignment of the center of the front and back faces of the tank were done by a precision alignment crew, who used the beam-darkened spots on the glass slides to locate the beam direction.

6. Water was added to the tank and the alignment was rechecked.

7. The plates were then added to the tank and the front and back plates were found to position exactly with the center of the front and back faces of the tank. The remaining plates were assumed to realign with the rest.

8. The tank was exposed to 6.15×10^9 electrons with a standard deviation of $\pm$ 1%.

9. The TL dosimeters (500 extruded rods and about 36 g powder) were read out on a Mark VI TLD reader.[10] The strings containing powder were cut off in small sections and the ^{7}LiF vibrated out, weighed, and then read out. The average dose values are tabulated for different positions (radii) in Table 1 and Table 2. The sections fitted into a geometrical pattern so that we could study beam profiles as a function of the azimuthal angle. The data was corrected for background and supralinearity using Fig. 3 and Ref. 7.

RESULTS AND DISCUSSION

Profile Measurements

Figure 5 shows the beam profile in two dimensions for the first detector plate. This plate was located at a depth of 0.05 radiation lengths and the dose profile should resemble very closely that of the actual beam profile. The histogram represents the dose evaluated from the extruded rods and the solid line represents the results from the glass plate exposure evaluated by a microdensitometer and normalized to the histogram. (Note: the glass plate did not have 0.05 radiation length in front of it.)

The elliptical beam spot is obvious both from the histogram and the glass plate. At larger radii and larger depths in the water tank the elliptical shape is essentially smeared out.

Equation (16) of Appendix A gives the absorbed dose in a LiF dosimeter (radius R) located at the center of the electron beam.

The quantity F in this formula is defined by Eq. (15) in Appendix A. For R = 0.5 mm (the radius of the extruded rods), a = 1.33 mm and b = 0.48 mm, the solution of Eq. (15) is F = 0.30.

Also,

$$N_e = 6.15 \times 10^9 \text{ electrons}$$

TABLE 1a

Average absorbed dose (rad) versus radius as measured with ^{7}LiF extruded rods for different detector plates (excepting plate 3).

Radius (mm)	Plate 1	Plate 2	Plate 4	Plate 6
0.00	10800.0		8400.0	12300.0
2.00	530.0	337.9	1195.5	1620.7
2.83	36.0	67.8	235.4	827.8
4.00	21.5	42.0	112.9	299.2
4.47	10.6	20.9	68.8	201.5
5.66	5.4	14.3	38.8	117.1
6.00	4.3	11.4	39.3	108.6
6.32	3.8	9.5	34.6	99.9
7.21	2.5	6.5	26.6	71.5
8.00	1.8	5.9	23.1	51.7
8.25	1.6	5.1	19.1	52.0
8.48	1.4	4.7	18.9	46.9
8.94	1.2	4.0	16.2	41.8
10.00	0.8	2.7	11.8	33.0
11.31	0.5	2.3	9.2	22.3
19.05		0.9	3.0	8.3
31.75		0.1	0.4	1.5
44.45			0.1	0.4
57.15				0.3
69.85				0.1
82.55				
95.25				0.1
107.95				
120.65				0.4
133.35				
152.40				
177.80				
203.20				
228.60				
254.00				
279.40				0.1

TABLE 1b

Average absorbed dose (rad) versus radius for plate number 3.

Radius (mm)	Plate 3
.71	4000.0
1.58	840.0
2.12	370.0
2.55	269.6
2.92	144.5
3.54	87.0
3.81	72.5
4.30	48.1
4.53	54.4
4.74	39.0
4.95	32.5
5.15	30.2
5.52	24.2
5.70	26.2
6.04	20.5
6.36	20.2
6.52	20.1
6.67	18.7
6.96	15.3
7.11	14.7
7.38	12.6
7.52	12.2
7.65	13.3
7.78	15.6
7.90	12.8
8.28	11.6
8.51	10.9
8.63	9.6
8.75	9.6
8.86	8.8
9.19	8.5
9.30	8.4
9.62	7.2
10.12	7.2
10.70	6.1
11.34	5.4
12.02	4.9
19.56	1.2
32.25	0.2
44.95	

TABLE 2

Average absorbed dose (rad) versus radius measured with ^{7}LiF powder for the different plates.

Radius (cm)	Plate 1	Plate 2	Plate 3	Plate 4	Plate 5	Plate 6
1.27	0.617±.038	2.612±.038	5.937±.232	11.249±.223	18.381±.397	27.208±.629
2.54	0.024±.001	0.256±.007	0.771±.027	1.691±.026	3.040±.063	4.470±.068
3.81	0.017±.002	0.051±.002	0.196±.008	0.455±.008	0.843±.013	1.300±.013
5.08	0.017±.002	0.014±.002	0.069±.002	0.168±.004	0.294±.005	0.471±.007
6.35	0.010±.002	0.009±.002	0.032±.002	0.079±.003	0.139±.003	0.202±.001
7.62	0.014±.003	0.006±.002	0.019±.002	0.048±.002	0.073±.002	0.100±.001
8.89	0.012±.002	0.005±.001	0.017±.001	0.034±.001	0.051±.002	0.059±.002
10.16	0.011±.001	0.002±.001	0.011±.002	0.023±.001	0.038±.001	0.041±.002
11.43	0.010±.001	0.002±.001	0.008±.002	0.017±.001	0.025±.001	0.030±.002
12.70	0.012±.001	0.008±.001	0.009±.002	0.016±.002	0.024±.002	0.024±.002
13.97	0.011±.001	0.010±.002	0.005±.001	0.015±.002	0.016±.002	0.020±.002
19.05	0.005±.001	0.003±.001	0.004±.001	0.009±.002	0.008±.002	0.010±.001
24.13	0.002±.001	0.002±.001	0.004±.001	0.003±.002	0.000±.001	0.005±.002
29.21	0.000±.002	0.000±.001	0.000±.001	0.000±.001	0.000±.001	0.000±.002

TABLE 3

Position of center of detector plates versus plate number.

Detector Plate Number	Depth in Tank (Z) cm
1	1.59
2	6.35
3	12.70
4	19.05
5	25.40
6	32.07

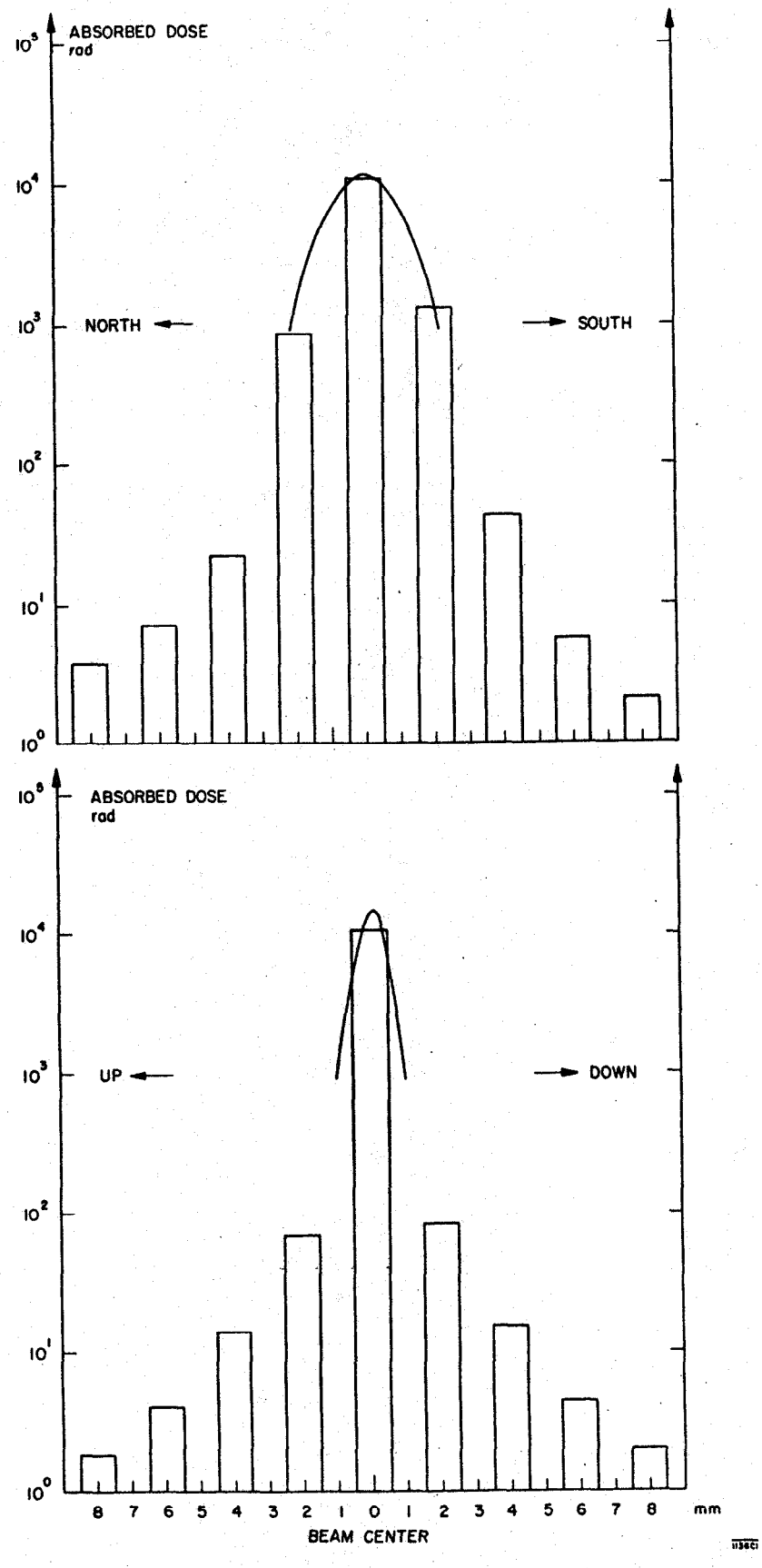

FIG. 5--Electron beam profile measured by ^{7}LiF extruded rods (histogram) for the first detector plate in the water tank. The solid lines represent glass plate exposures (taken in front of the tank) normalized to ^{7}LiF data. Top curve: Horizontal profile. Bottom curve: Vertical profile.

and

$$\left(\frac{1}{\rho}\frac{dT}{dx}\right)_{LiF}^{10\ GeV} = 2.11\ \left[MeV\ cm^2\ g^{-1}\right]^{11} ,$$

so that Eq. (16) gives

$$D^{rod} = 7.90 \times 10^3\ rad\ .$$

The measured value in the center rod of the first plate (see Table 1) is 1.08×10^4 rad. The calculated value is 27% lower than the measured value. In view of the uncertainties in the dosimetry, this discrepancy is not too serious.

Figures 6 to 11 show the beam profiles in terms of absorbed dose for the different plates. The histogram represents the rod data from the array in the center and a few lateral rod positions of the detector plates. All the dose values at a given distance from the center rod have been averaged over the azimuthal angle and plotted as a function of distance from the center (see also Table 1). As pointed out earlier, plate #3 is an exception because of a misalignment. Figures 8 and 9 show the uncorrected and corrected data respectively. The dose data from each polyethylene tubing containing ^{7}LiF powder was averaged and Fig. 12 shows a plot of dose as a function of radius for plates 1 to 6. The part of the curves between zero and 12.5 mm consists of rod data (the same as Figs. 6 to 11) beyond 12.5 mm, the curves consist of powder data. In detector plate 5, no array of extruded rods was available. An interesting detail is that the dose on plate 1 for radii above 60 mm is higher than for plates 2 and 3b. A possible explanation is that particles with very low penetrative power, e.g., delta-rays produced in the beam exit windows and the air, might contribute to the dose on the first plate only.

Depth Measurements

The Monte Carlo calculations by Alsmiller and Beck are represented by the histogram in Fig. 13, which plots D_r/ϕ where D_r and ϕ are defined in Appendix A. The geometry is that of a broad beam of monoenergetic electrons incident on a semi-infinite slab of water. Photons with energies less than 10 keV and electrons and positrons with energies less than 2 MeV were assumed to deposit their energy locally in both calculations. One significant difference between Alsmiller's and Beck's Monte Carlo code is that the latter has included the correction for density effect in the stopping power.[3] The corresponding reduction in stopping power gives a lower absorbed dose rate per unit flux density.

The same quantity as calculated by Alsmiller and Beck can be derived from the measured dose distribution. Equation (21) in Appendix A gives

$$\frac{D_r}{\phi} = 3.68 \times 10^{-6} \int_0^\infty r\ \bar{B}(z,r)\ dr$$

where $\bar{B}(z,r)$ is the absorbed dose distribution plotted in Figs. 6 to 11 for the different detector plates (depth z). Table 3 shows the depth of the center of each plate versus plate number. By drawing smooth curves through these histograms, $r\bar{B}(z,r)$ can be calculated and plotted as a function of r. The smooth curves through the histograms of $\bar{B}(z,r)$ were easily drawn by eye for plates 3b, 4 and 6. The error bars on these triangles represent two extreme ways of drawing the smooth curve. The center rod was missing in plate 2; however, the dose at the center of the adjacent plates (i.e., that is, 1 and 3b) differed by only 25%. Therefore, a linear interpolation between these values was used for the center dose value of plate 2. For plate 1, a gaussian-shaped curve (see Eq. (13) and the beam profile discussion in Appendix A) was used out to a distance of $r = 0.75$ mm and thereafter the curve was drawn by eye.

Graphical integration yielded the integral in Eq. (21) (Equation above). The integration was never carried out further than 35 mm. The triangles in Fig. 13 show the results of the

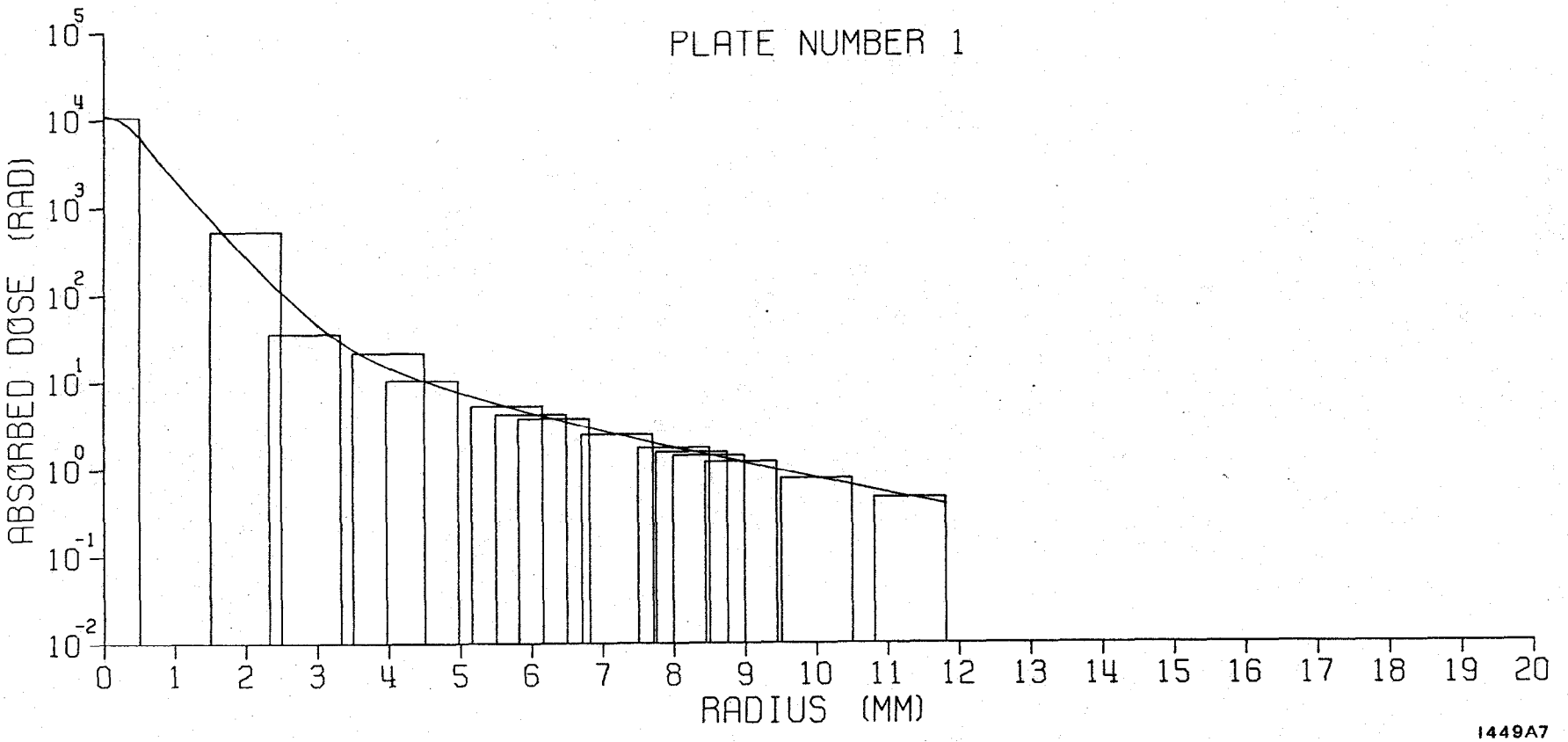

FIG. 6--Beam profile in terms of absorbed dose (rad) measured with ^{7}LiF extruded rods. The histogram represent dose values averaged over the azimuthal angle. The smooth curve has been drawn using technique described in text. The data are listed in Table 1a.

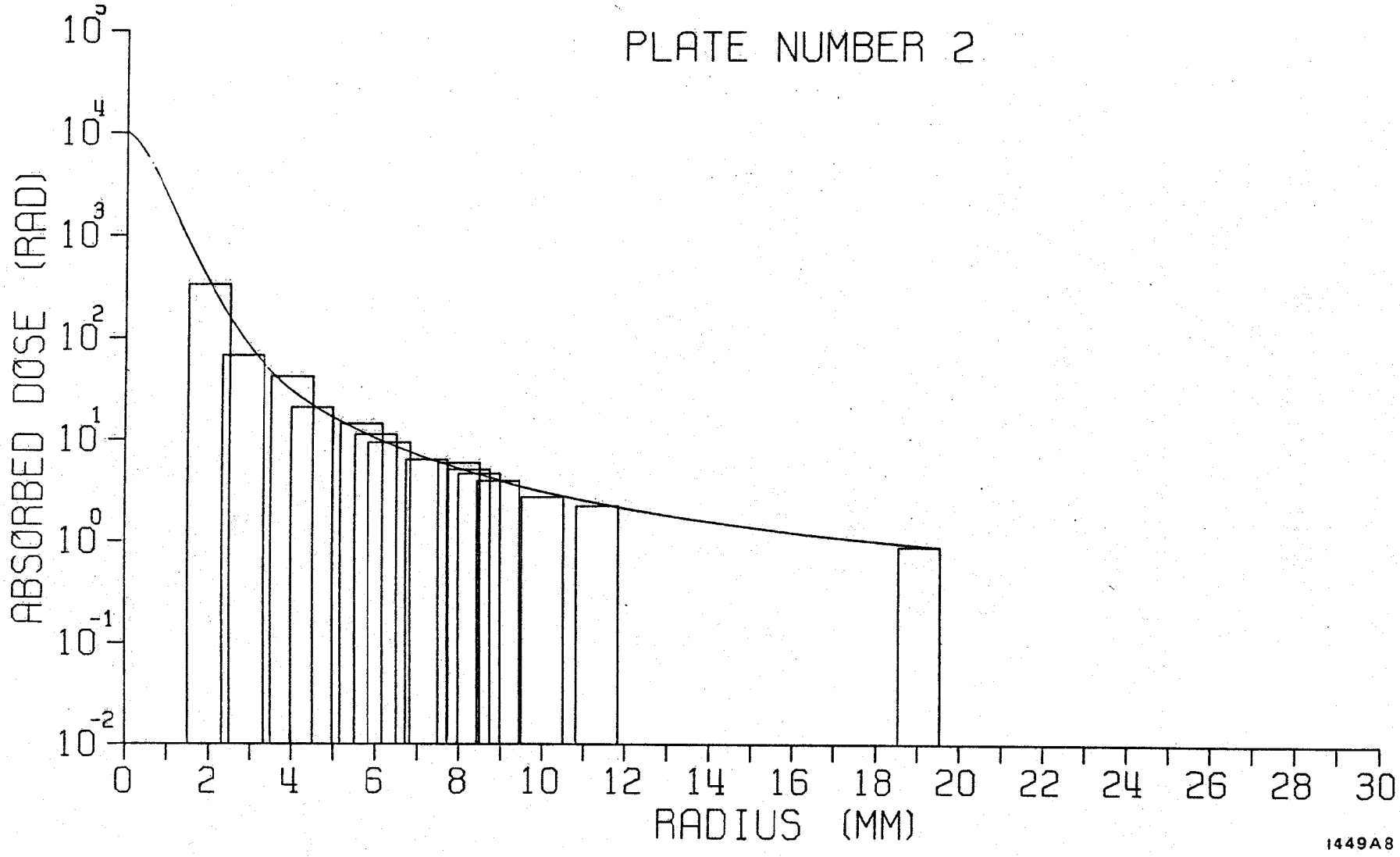

FIG. 7--Beam profile in terms of absorbed dose (rad) measured with ^{7}LiF extruded rods. The histogram represent dose values averaged over the azimuthal angle. The smooth curve has been drawn using technique described in text. The data are listed in Table 1a.

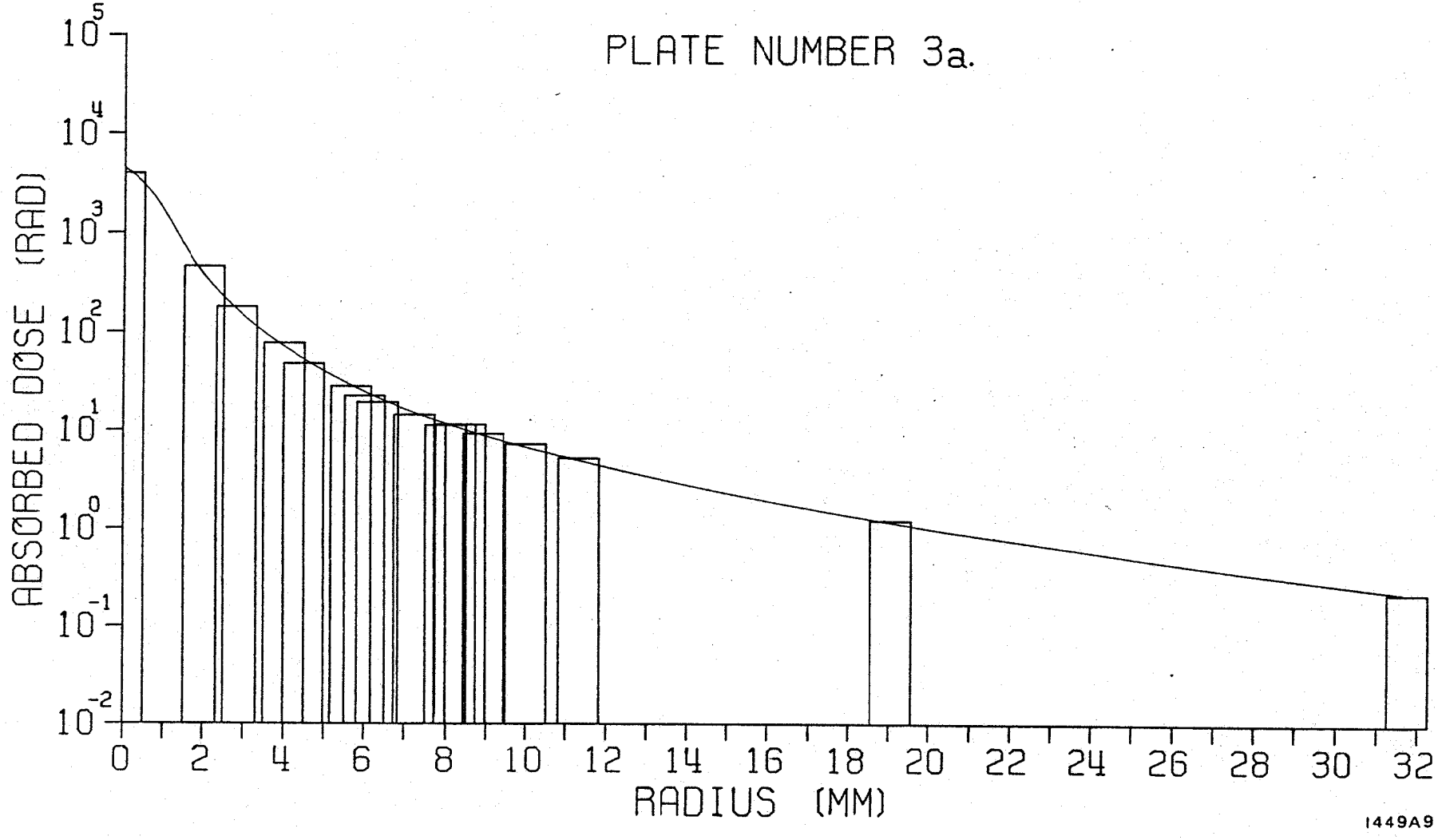

FIG. 8--Beam profile without correction for misalignment in terms of absorbed dose (rad), measured with ^{7}LiF extruded rods. The histogram represent dose values averaged over the azimuthal angle. The smooth curve has been drawn using technique described in text. The data are listed in Table 1a.

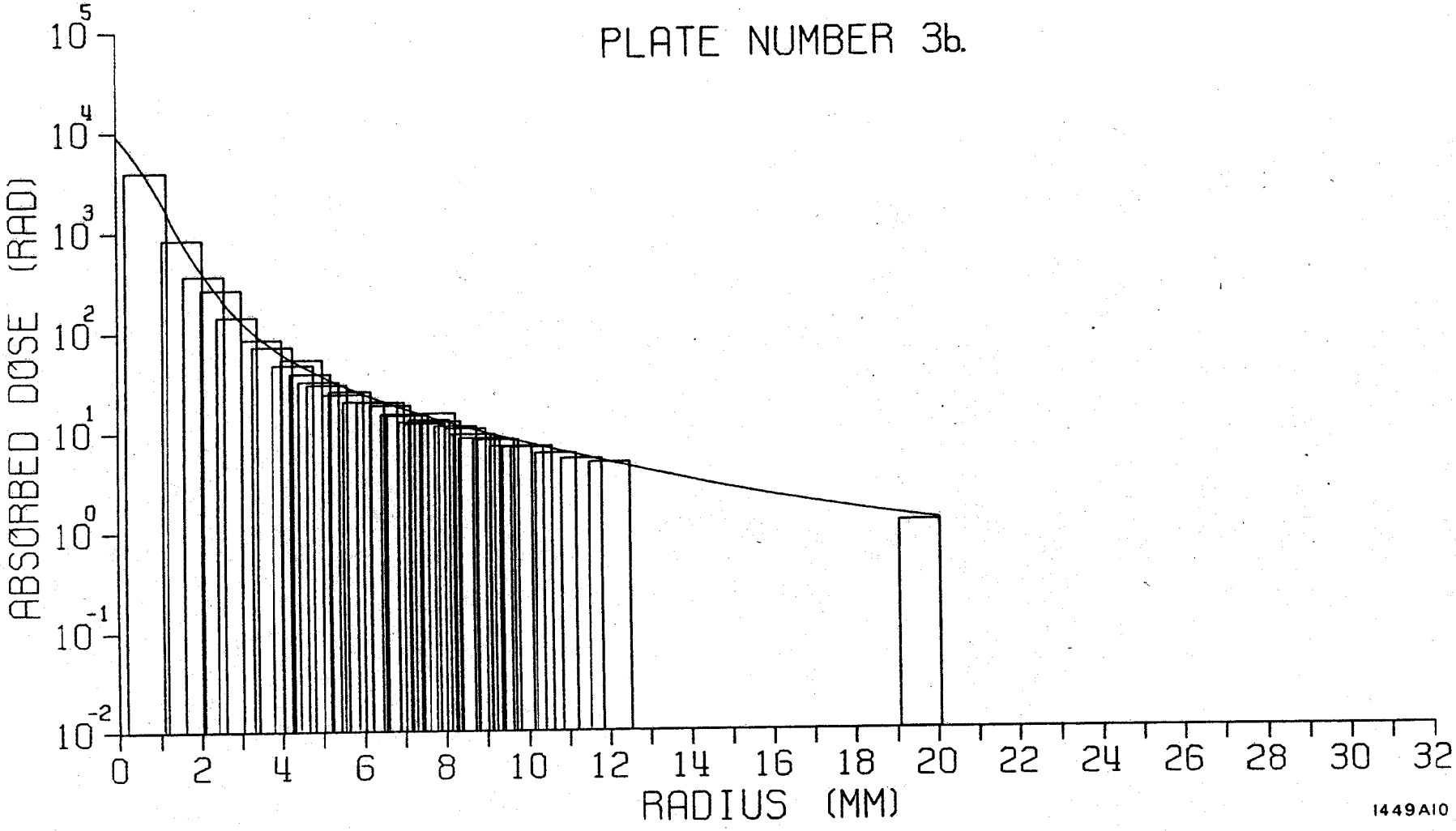

FIG. 9--Beam profile with correction for misalignment in terms of absorbed dose (rad), measured with ^{7}LiF extruded rods. The histogram represent dose values averaged over the azimuthal angle. The smooth curve has been drawn using technique described in text. The data are listed in Table 1b.

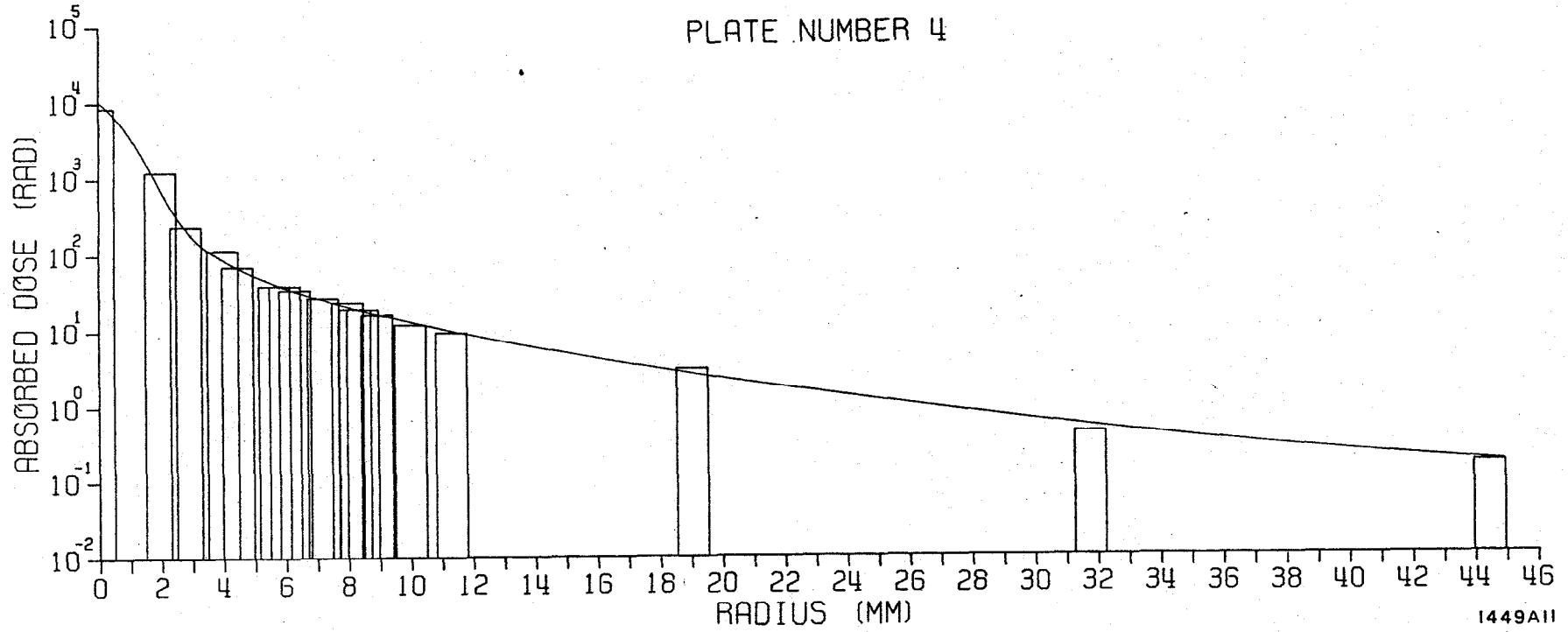

FIG. 10--Beam profile in terms of absorbed dose (rad) measured with ^{7}LiF extruded rods. The histogram represent dose values averaged over the azimuthal angle. The smooth curve has been drawn using technique described in text. The data are listed in Table 1a.

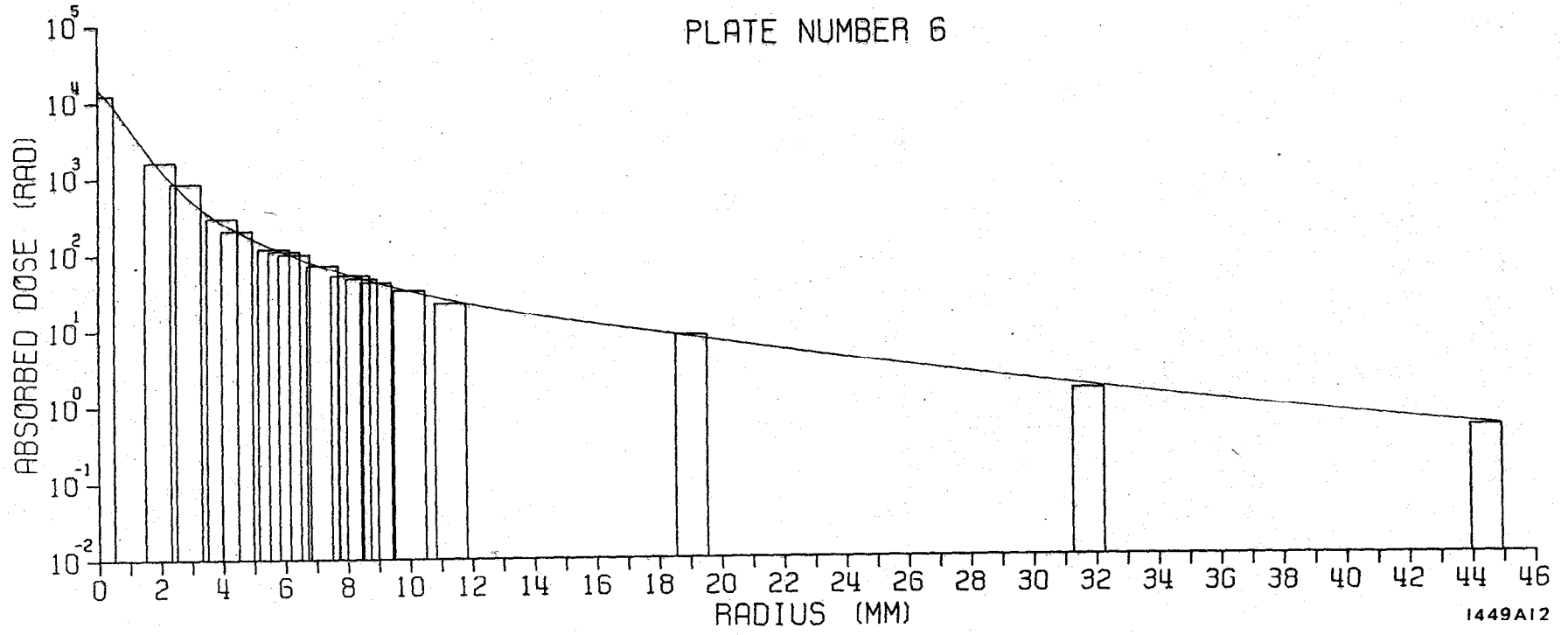

FIG. 11--Beam profile in terms of absorbed dose (rad) measured with ^{7}LiF extruded rods. The histogram represent dose values averaged over the azimuthal angle. The smooth curve has been drawn using technique described in text. The data are listed in Table 1a.

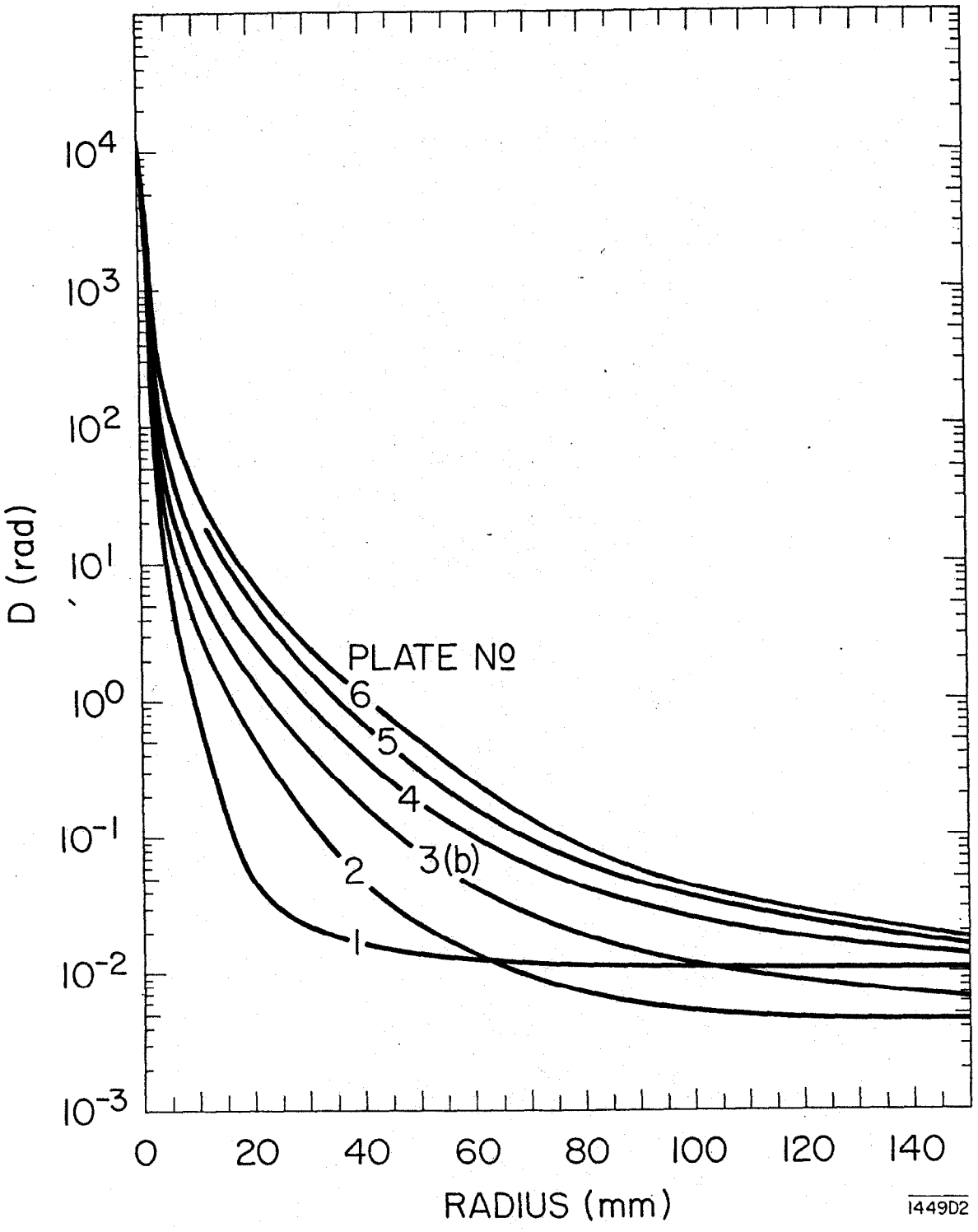

FIG. 12--Radial dose distribution for the different detector plates. The data from the ^{7}LiF extruded rods, as well as from the ^{7}LiF powder, was averaged over azimuthal angle. The overlapping region (radius ~10 mm), where both rods and powder were used, show perfect agreement between the two types of dosimeters.

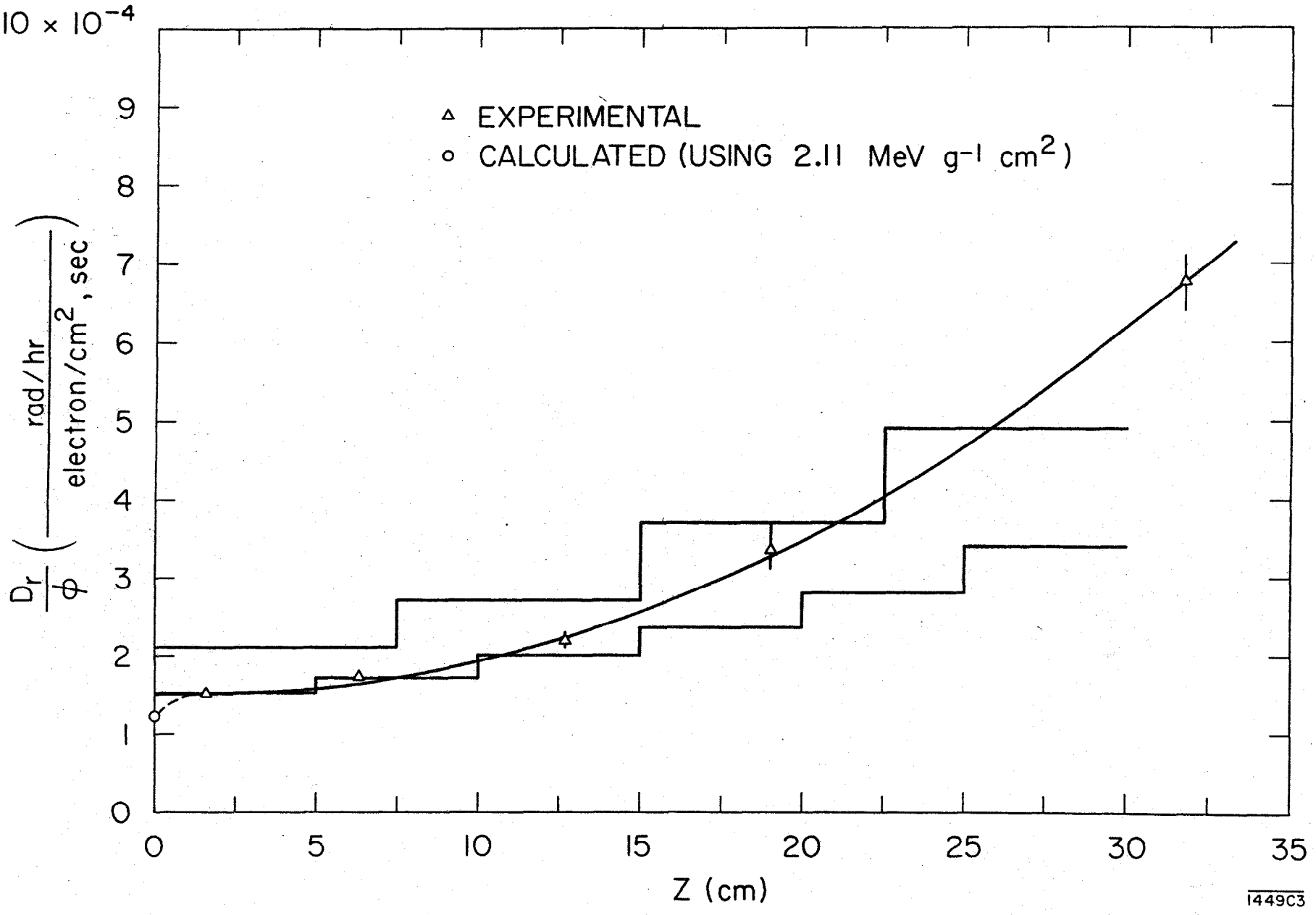

FIG. 13--Dose rate at maximum per incoming unit electron flux density $D_r(z)/\phi$ [rad hr^{-1} cm^2 sec]. Top histogram represents the Monte Carlo calculations of Alsmiller;[2] bottom histogram that of Beck.[3] The curve is a second order polynomial least square fit to the experimental points.

graphical integration for different depths. The solid line through the triangles in Fig. 13 is a least square fit to a second order polynomial of the form $y = a_0 + a_1 + a_2x^2$.*

The open dot is calculated by a transformation of collision mass stopping power $(dT/\rho\,dx)^{E}_{M}$ into appropriate units:

$$\frac{D_r}{\phi} = \left(\frac{dT}{\rho dx}\right)^{10}_{LiF} \left[\frac{MeV\ cm^2}{g}\right] 1.60 \times 10^{-6} \left[\frac{erg}{MeV}\right] 3.60 \times 10^{3} \left[\frac{sec}{h}\right] 10^{-2} \left[\frac{rad,\ g}{erg}\right]$$

$$= \left(\frac{dT}{\rho dx}\right)^{10}_{LiF} \times 5.76 \times 10^{-5}$$

As before, we chose $(dT/\rho dx)^{10\,GeV}_{LiF} = 2.11$ MeV $cm^2 g^{-1}$ and $D_r/\phi = 1.21 \times 10^{-4}$ rad hr^{-1} cm^2 sec.

Figure 13 shows that there is an excellent agreement between Beck's data and our measurement at small depths. At larger depths the measurements approach Alsmiller's histogram (calculated without density effect). The sharp buildup of the measured curve in comparison with Beck's calculations is not understood. A significant photon beam could give this effect. Although other SLAC experimenters have observed a small photon contamination, the qualitative and quantitative arguments given in Appendix B indicate that the effect can be explained if a 0.3 radiation length target is assumed to intercept the electron beam. Photon contamination corresponding to such a thick target is not possible with the experimental arrangements used in our experiment, and the discrepancy between Beck's histogram and our measurements requires other explanations.

Figure 14b shows the maximum absorbed dose in a 25 cm deep water tank, per incident electron fluence, D/ψ, as a function of the incident electron energy. This is essentially the reciprocal of the quantity plotted in the papers by Alsmiller and Tesch. The calculations by Alsmiller and Beck are plotted together along with two experimental points — this experiment at 10 GeV and Tesch's at 5.2 GeV. The curve illustrates the good agreement between this experiment and Alsmiller's data at 25 cm depth. The high value of Tesch's is explained by him as photon contamination of the electron beam.

In the energy region below 50 MeV the maximum dose is very close to the surface dose (< 8%).[15] That is, there is no significant buildup of dose contributing secondary particles. The maximum dose per electron fluence, D/ψ, is therefore related to the mass collision stopping power, $(dT/\rho\,dx)^{E}_{H_2O}$, for the primary electrons. Between 10 and 50 MeV, $(dT/\rho\,dx)^{E}_{H_2O}$ varies only 7%,[2] so the quantity D/ψ is an essential constant in this region and equal to

$$2.0 \left(MeV \frac{cm^2}{g}\right) \times 1.6 \times 10^{-6} \left(\frac{erg}{MeV}\right) \times 10^{-2} \left(\frac{rad\ g}{erg}\right) = 3.2 \times 10^{-8}\ rad\ cm^2$$

Around the critical energy† (92 MeV for water) the electromagnetic shower will cause a significant multiplication of particles at larger depths in the water tank. This causes the maximum dose per electron fluence, D/ψ, to increase with increasing energy. These effects are seen in Fig. 14b.

Integral Dose

The total energy (g rad) absorbed in the tank of water (per electron) can be calculated by integrating the depth-dose curve over the total tank depth. Quite often, for low

*A least square fit computer program was written using the numerical technique suggested by Milne.[14]

†The critical energy is defined as the electron energy at which the collision loss is equal to the radiation loss.

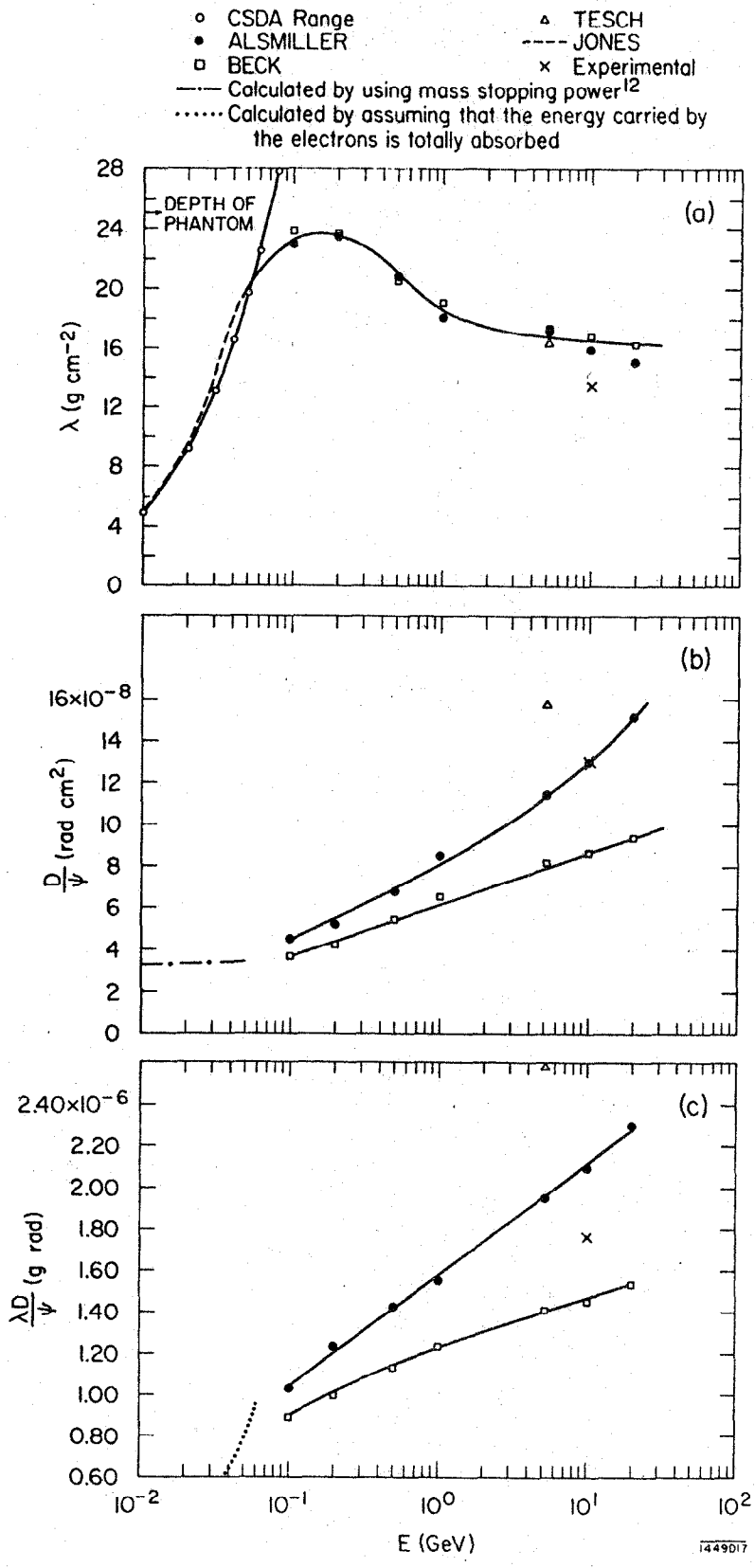

FIG. 14--All solid lines are drawn by eye; all curves represent the results for a 25 cm water phantom. (a) Integral dose per absorbed dose at maximum for a beam size of 1 cm^2, $\lambda(E)$. The radiological unit is [g rad/rad cm^2]. The dimension is distance with the unit [g cm^{-2}]. (b) Absorbed dose at maximum per incoming unit electron fluence $(D/\psi)(E)$ [rad cm^2]. (c) Integral dose per incoming electron, $(\lambda D/\psi)(E)$, [g rad].

energies,[15] the energy thus obtained is divided by the maximum dose per electron fluence, D/ψ, and the resulting quantity has units of areal density (g cm^{-2}). This quantity, λ, is shown in Fig. 14a as a function of the incident electron energy (see Appendix A, Eq. (24)).

The total energy per electron, $D\lambda/\psi$, often called the integral dose, is given in Fig. 14c as a function of energy. In the low energy region (i.e., below 50 MeV) the electrons are completely stopped in 25 cm of water, so that except for a small correction for bremsstrahlung losses, the total energy is equal to the incident energy. Therefore the integral dose per electron, $D\lambda/\psi$, is a linear function of the incident electron energy as indicated by the dotted line in Fig. 14c. In the region of 80-100 MeV, the projected range of the electrons becomes larger than the thickness of the water phantom and the radiation losses start to become significant. Therefore, the slope of the curve is smaller than in the low energy region.

The quantity λ is obtained from the ratio of the ordinates of Figs. 14b and 14c, and the maximum thus obtained is due to the changes in the two curves at 100 MeV (Fig. 14b was discussed above).

Below 100 MeV, as previously discussed, much of the energy is absorbed in a 25 cm thick water slab. The quantity λ should therefore resemble the total path-length of the electrons in water. This is shown in Fig. 14a, where the broken line is the integral dose as calculated by Jones[15] using average stopping powers (including density effect) and compared to the CSDA* range.

There is little information in the literature about the correlation of integral dose and radiation effects. H. E. Johns[16] discusses the integral dose concept and concludes that it can be used as a rough guide to constitutional effects to be expected following irradiation. If the integral dose is to be regarded as an important factor in the judgement of radiation damage, there may be an inconsistency in the present use of absorbed dose (or dose equivalent) to specify acceptable radiation levels because λ varies considerably with energy. The majority of electron accelerators operate with energies $\leq$ 100 MeV,[20] where λ has its strongest variation (λ varies a factor of five from 10 to 100 MeV). Thus the energy spectrum of the electrons is quite important.

The discussion so far has been concerned with broad beam situations, that is, irradiation conditions, whereby the irradiated object is small in comparison with the radiation field. In the use of accelerators for high energy physics, the beam is usually collimated and focussed so that it resembles a delta-function. At SLAC, the health physicist has to face the possibility of a person being accidentally irradiated by an electron or positron beam of this kind, as well as to the more common whole body type irradiation. In this experiment, 95% of the absorbed energy was deposited within a frustrum having a radius of 0.15 cm at the beam entrance and 1.75 cm at the beam exit (the total water mass of this frustrum was 96 g). Using 70 kg as the mass of a standard man, it is easy to show that under the assumption that the energy deposited outside the frustrum was uniformly deposited, the ratio of the <u>average</u>† dose outside the frustrum to the <u>average</u> dose inside is 7×10^{-5}. The conclusion is that the dose to the whole body under such condition (small, localized beam) is of secondary importance.

An experiment was recently performed at SLAC in order to study the biological effects in rats exposed to intense, small electron beams.[16] A dose of about 10^7 rad was given to the thigh of a rat using a 2 mm by 4 mm electron beam. Although gross anomalies were seen where the beam hit, the whole body dose was low enough so that the rat seemed to be in a healthy condition after one week, at which time it was sacrificed for cell damage studies.

*Continuous slowing down approximation.[12]
†Average dose means energy absorbed in a given mass, divided by that mass.

Summary

The dose buildup due to the development of the electromagnetic cascade has been studied in a 0.8 radiation length thick lucite-water tank with a 10 GeV well-focussed electron beam. The dosimetry used was thermoluminescent ^{7}LiF. It was assumed that the dosimeters measured absorbed dose fairly accurately although this is a statement which needs to be proved by using absolute methods. The buildup curve was compared with two different Monte Carlo calculations[2, 3] and agreed with one[2] at small depths and with the other[1] at larger depths. The concept of integral dose and its significance for the interpretation of maximum permissible radiation levels for high energy electrons was discussed. For electrons with energies above 1 GeV the integral dose was about three times higher than for electrons with energies below 10 MeV, for the same maximum absorbed dose.

The average whole body dose versus peak dose in a small intense electron beam was discussed and illustrated by reporting preliminary observations from a recent animal experiment at SLAC.

Acknowledgements

The authors wish to express their gratitude to Mr. Ted Jenkins for helping with the experimental setup and exposures. We are grateful to Miss Debbie Peckham for reading the thermoluminescent dosimeters and for general technical assistance. The SLAC Health Physics and operating groups, particularly the precision alignment crew, were very helpful during the initial phases of the experiment. Discussions with Dr. R. G. Alsmiller, Jr. (ORNL) and Mr. Harold Beck (HASL) concerning calculated results are appreciated.

References

1. K. Tesch, Dosisleistung und Toleranzflussdichte Hochenergetischer Elektronen- und Gammastrahlen, Nukleonik, 8: 264-266 (1966).

2. R. G. Alsmiller, Jr. and H. S. Moran, Dose Rate from High Energy Electrons and Photons, Nuclear Instruments and Methods, 58: 343-344 (1968).

3. H. Beck, Health and Safety Laboratory, New York, Personal Communication 1969 .

4. W. R. Nelson, T. M. Jenkins, R. C. McCall, and J. K. Cobb, Electron-Induced Cascade Showers in Copper and Lead at 1 GeV, Phys. Rev., 149: No. 1, 201-208 (1966).

5. F. H. Attix and W. C. Roesch (Ed.), Radiation Dosimetry, Vol. 1, 2nd ed., pp. 363-380, Academic Press, New York, 1968.

6. H. DeStaebler, Jr., Transverse Radiation Shielding for the Stanford Two-Mile Accelerator, USAEC Report SLAC-9, pp. 2-5, Stanford Linear Accelerator Center, Nov. 1962.

7. R. C. Fix of Tracerlab, LFE and R. C. McCall of Stanford Linear Accelerator Center, Personal Communication, 1969.

8. G. E. Fischer, Electron Beam Profile Measurements, Rev. Sci. Instr., 35: No. 8, 1081 (1964).

9. R. S. Larsen, and D. Horelick, A Precision Toroidal Charge Monitor for SLAC in Symposium on Beam Intensity Measurement, Daresbury, April 22-26, 1968, Report DNPL/RI, pp. 260-279, 1968.

10. R. C. McCall and G. Babcock, Stanford Linear Accelerator Center, Personal Communication, 1969.

11. W. R. Nelson, Stanford Linear Accelerator Center, Unpublished Calculation of Stopping Power for Electrons Extended to 100 GeV, Using Formulas from Berger and Seltzer,[12, 13] 1969.

12. M. J. Berger and S. M. Seltzer, Tables of Energy Losses and Ranges of Electrons and Positrons, Report NASA SP-3012, National Bureau of Standards, Washington, D.C., 1964.

13. M. J. Berger and S. M. Seltzer, Additional Stopping Power and Range Tables for Protons, Mesons and Electrons, Report NASA SP-3036, National Bureau of Standards, Washington, D.C., 1966.

14. W. E. Milne, Numerical Calculus, 6th Printing, pp. 242-250, Princeton University Press, Princeton, New Jersey, 1962.

15. J. C. Jones, Integral Dose in Electron Therapy in Symposium on High Energy Electrons, Montreux, Switzerland, September 7-11, 1964, A. Zuppinger and G. Poretti (Ed.), pp. 71-76, Springer-Verlag, New York, 1965.

16. H. E. Johns, The Physics of Radiology, 2nd ed., pp. 353-357, Charles C. Thomas, Springfield, Illinois, 1961.

17. G. K. Svensson, R. C. McCall, T. M. Jenkins, and W. R. Nelson, Stanford Linear Accelerator Center, Use of Thermoluminescent Dosimeters in High Energy Health Physics in Second International Conference on Luminescence Dosimetry, Gatlinburg, Tennessee, September 23-26, 1968, USAEC, ORNL Report TID-4500, pp. 737-750, 1968.

18. R. C. McCall of Stanford Linear Accelerator Center, L. Sagan of Palo Alto Medical Clinic, K. Bensch of Stanford University Medical School, and D. D. Busick of Stanford Linear Accelerator Center, Personal Communication, 1969.

19. R. G. Jaeger, E. P. Blizard, A. B. Chilton, M. Grotenhuis, A. Hönig, Th. A. Jaeger, and H. H. Eisenlohr (Ed.), Engineering Compendium on Radiation Shielding, Vol. I, p. 13, Springer-Verlag, New York, 1968.

20. E. A. Burrill, The Expanding Use of Particle Accelerators in Research, Medicine and Industry: A Statistical Review to be presented at The Second International Conference on Accelerator Dosimetry and Experience, November 5-7, 1969, Stanford Linear Accelerator Center, Stanford, California.

Symbols

$\psi(r,\theta) = \frac{d^2n}{rdrd\theta}$	=	Differential number of electrons (cm^{-2}) at a distance (r,dr) from origin at an angle (θ,dθ) in the (z=0) plane (referred to as electron fluence).
ϕ	=	Incident electron flux density (cm^{-2} sec).
$B(z,r,\theta)$	=	Absorbed dose (rad) in a mass element $\Delta m = \rho \Delta v$ where the volume element is located at radius (r, Δr) at angle (θ, $\Delta\theta$) from origin, at depth (z, Δz) from the surface of the water tank.
$\bar{B}(z,r)$	=	Absorbed dose (rad) averaged over azimuthal angle θ.
D	=	Absorbed dose at dose maximum in the water tank.
D^{rod}	=	Average absorbed dose in center rod for plate number 1.
$D_r(z)$	=	Dose rate at depth z in the water tank (rad hr^{-1}).
E_0	=	Total electron energy.
$\left(\frac{dT}{\rho dx}\right)_M^E$	=	Collision mass stopping power for material M at energy E taken from Refs. 11, 12, or 13.
r	=	Distance from beam center to any point in the z plane.
z	=	Depth in the water tank.
N_e	= =	Total number of electrons impinging on the water tank, $6.15 \times 10^9 \pm 1\%$.
F	=	The fraction of the total number of electrons incident within the distance r=R from the origin.

Beam Profile Considerations

The electron beam spot appeared to be elliptical. Assume that it has a profile of gaussian shape along either semi-axis. That is $\psi(r,\theta)$ is of the form

$$\psi(r,\theta) = \frac{d^2n}{rdrd\theta} = C\, e^{-f(r,\theta)} \tag{1}$$

where

$$f(r,\theta) = \frac{r^2}{(r')^2} \tag{2}$$

C = normalization constant

$$(r')^2 = \frac{a^2b^2}{a^2 \sin^2\theta + b^2 \cos^2\theta} \tag{3}$$

This is the polar equation of an ellipse with origin in the center.

a = semimajor axis at 1/e from peak value

b = semiminor axis at 1/e from peak value

Averaging over θ gives

$$\bar{\psi}(r) = \frac{\int_0^{\pi/2} C\, e^{-f(r,\theta)}\, d\theta}{\int_0^{\pi/2} d\theta} = \frac{2C}{\pi} \int_0^{\pi/2} e^{-f(r,\theta)}\, d\theta \tag{4}$$

Substitute (3) into (2)

$$f(r,\theta) = \frac{r^2}{a^2 b^2}(a^2 \sin^2\theta + b^2 \cos^2\theta)$$

$$= \frac{r^2(a^2-b^2)}{2a^2b^2} - \frac{r^2(a^2-b^2)\cos 2\theta}{2a^2b^2} + \frac{r^2}{a^2} \tag{5}$$

Define two quantities

$$P = \frac{r^2}{2a^2b^2} \tag{6}$$

and

$$P' = \frac{r^2}{2a^2b^2}(a^2-b^2) = P(a^2-b^2) \tag{7}$$

Let

$$x = 2\theta \tag{8}$$

$$\therefore \quad dx = 2d\theta$$

Substitute (6), (7), and (8) into (5)

$$f(r,\theta) = -P' \cos x + \frac{r^2}{a^2}\left[1 + \frac{1}{2}\left(\frac{a^2-b^2}{b^2}\right)\right]$$

$$= -P' \cos x + (a^2+b^2)P \tag{9}$$

Equations (4) and (9) give

$$\bar{\psi}(r) = \frac{C}{\pi} e^{-(a^2+b^2)P} \int_0^{\pi} e^{P' \cos x}\, dx \tag{10}$$

The integral in Eq. (10) can be written in the form of a Bessel function $I_0(P')$ of degree n=0 and with the argument

$$P' = \frac{r^2}{2a^2b^2}(a^2-b^2)$$

so that

$$\int_0^{\pi} e^{P' \cos x}\, dx = \pi I_0(P')$$

and

$$\overline{\psi}(r) = C\, e^{-(a^2+b^2)P}\, I_0(P') \tag{11}$$

The electron fluence

$$\psi(r,\theta) = \frac{d^2n}{rdrd\theta}$$

multiplied by the area $rdrd\theta$ and integrated over θ and r will give the total number of electrons (N_e). Thus C is defined by (see Eq. (1))

$$N_e = 4C \int_0^{\infty} \int_0^{\pi/2} e^{-f(r,\theta)}\, rdrd\theta$$

$$= 2\pi C \int_0^{\infty} r\, e^{-(a^2+b^2)P}\, I_0(P')\, dr \tag{12}$$

Combining Eqs. (11) and (12) give

$$\overline{\psi}(r) = \frac{N_e\, e^{-(a^2+b^2)P}\, I_0(P')}{2\pi \int_0^{\infty} r\, e^{-(a^2+b^2)P}\, I_0(P')\, dr} \tag{13}$$

This equation has been solved for a = 1.33 mm and b = 0.48 mm and it has been used as a shape function in order to draw a smooth curve through the histogram of detector plate #1. The assumption then is that the electron fluence $\overline{\psi}(r)$ is proportional to the absorbed dose, that is $B(z=0,r) = \text{const.}\ \overline{\psi}(r)$. The total number of electrons is given by Eq. (12). The number of electrons incident within the radius R is

$$2\pi C \int_0^{R} r\, e^{-(a^2+b^2)P}\, I_0(P')\, dr$$

The fractional number of electrons (F) incident within the radius R is given by

$$F = \frac{2\pi C \int_0^{R} r\, e^{-(a^2+b^2)P}\, I_0(P')\, dr}{N_e} \tag{14}$$

Equations (12) and (14) give

$$F = \frac{\int_0^{R} r\, e^{-(a^2+b^2)P}\, I_0(P')\, dr}{\int_0^{\infty} r\, e^{-(a^2+b^2)P}\, I_0(P')\, dr} \tag{15}$$

A rod dosimeter in the electron beam center covering an area of πR^2 should receive the average absorbed dose of

$$D^{rod} = \frac{FN_e}{\pi R^2} \left(\frac{dT}{\rho dx}\right)^E_{LiF} 1.6 \times 10^{-8} \text{ rad} \tag{16}$$

Note: Due to an algebraic mistake in an earlier publication,[17] $I_0(P')$ was written $I_0(P)$. This created a 30% higher value of F in our application.

Calculation of Integral Dose

All experimental dose values used in calculations have been averaged over the azimuthal angle θ. Derivations are done for a constant electron energy, E. Definition of absorbed dose (rad)

$$\bar{B}(z,r) = \frac{\Delta T}{\Delta m} = \frac{\Delta T}{\rho \Delta v} \tag{17}$$

where

$$\Delta v = 2\pi \, r \, dr \, \Delta z$$

$$dT = 2\pi \, \rho \Delta z \, \bar{B}(z,r) \, r \, dr \tag{18}$$

The total energy absorbed in the plane $(z, \Delta z)$ is

$$T(z) = 2\pi \rho \Delta z \int_0^\infty \bar{B}(z,r) \, r \, dr \quad \overline{g \text{ rad}} \tag{19}$$

For an infinitely broad beam, that is no energy escapes laterally, Eq. (19) can be used to calculate the average dose in the plane $(z, \Delta z)$ per unit incident electron fluence

$$\frac{\bar{B}(z)}{\psi} = \frac{T(z)}{N_e \rho \Delta z} \left[\frac{\text{g rad cm}^2}{\text{g}}\right]$$

$$= \frac{2\pi}{N_e} \int_0^\infty r \, \bar{B}(z,r) \, dr \quad [\text{rad cm}^2] \tag{20}$$

$\bar{B}(z,r)$ is the absorbed dose plotted in Figs. 6 to 12. By applying a time factor to Eq. (20) the quantity plotted in Fig. 13 is given by

$$\frac{D_r}{\phi} = \frac{D_r(z)}{\phi} = \frac{\bar{B}(z) \; 3.6 \times 10^3}{\psi}$$

$$= \frac{2\pi \; 3.6 \times 10^3}{6.15 \times 10^9} \int_0^\infty r \, \bar{B}(z,r) \, dr$$

$$= 3.68 \times 10^{-6} \int_0^\infty r \, \bar{B}(z,r) \, dr \quad [\text{rad hr}^{-1} \text{ cm}^2 \text{ sec}] \tag{21}$$

The experimental and calculated values of D_r/ϕ have been fitted to second order polynomials (see text) by a least square technique.[14]

At a certain $z=z_m$, $\bar{B}(z)$ has a maximum value, and $D = \bar{B}(z_m)$ [rad]. D/ψ is plotted in Fig. 14b as a function of electron energy.

The total energy deposited in the water tank is given by integrating Eq. (19) over depths z,

$$T = \int_0^{25} T(z)\, dz \quad [\text{g rad}]$$

The energy absorbed per electron is

$$\frac{T}{N_e} = \frac{\int_0^{25} T(z)\, dz}{N_e} \quad [\text{g rad}] \tag{22}$$

This quantity is usually normalized to the maximum dose per electron fluence D/ψ [rad cm^2] (plotted in Fig. 14b) and this gives the quantity

$$\lambda = \frac{T\psi}{N_e D} = \frac{\psi \int_0^{25} T(z)\, dz}{N_e D} \quad \left[\frac{\text{g rad}}{\text{rad cm}^2}\right] \tag{23}$$

or [g cm^{-2}].

Equation (20) and (23) gives

$$\lambda = \frac{\rho \int_0^{25} \bar{B}(z)\, dz}{D} \tag{24}$$

As mentioned earlier Eq. (21) has been fitted to a second order polynomial so the solution of Eq. (24) is trivial. λ as a function of E is plotted in Fig. 14a. The quantity in Fig. 14c is defined by Eq. (22) and is easily calculated by multiplying λ and D/ψ.

$$\frac{\lambda D}{\psi} = \frac{T}{N_e} = \frac{\int_0^{25} T(z)\, dz}{N_e} \quad [\text{g rad}] \tag{25}$$

APPENDIX B

This appendix will discuss qualitatively and quantitatively the effect of a photon-contamination of the electron beam.

1. The first consideration concerns the exit window and airpath upstream of the water tank. The total thickness of material corresponds to 10^{-2} radiation lengths. The electron current was measured in a toroid located further upstream (Fig. 4). The only effect of the exit window and airpath will be a displacement $\Delta z = -10^{-2}$ radiation lengths (3.7 mm H_2O) for the calculated curve.

Clearly the source of photons must be located at some distance upstream from the toroid.

2. Calculation of the thickness of the converter necessary to give the observed discrepancy between Beck's calculation and this experiment at large depths. The symbols used are valid for this appendix only.

Let

$D(z)$ = absorbed dose rate from electrons and photons at depth z $[\text{rad hr}^{-1}]$

$D_\gamma(z)$ = absorbed dose rate from photons at depth z $[\text{rad hr}^{-1}]$

$D_e(z)$ = absorbed dose rate from electrons at depth z $[\text{rad hr}^{-1}]$

$$D(z) = D_\gamma(z) + D_e(z) \tag{1}$$

$B_\gamma(z,k)$ = absorbed dose rate as calculated by Beck per unit photon flux density for photons of energy (k, dk) $[\text{rad hr}^{-1}\ \text{cm}^2\ \text{sec}]$

$B_e(z)$ = absorbed dose rate as calculated by Beck per unit electron flux density for 10 GeV electrons $[\text{rad hr}^{-1}\ \text{cm}^2\ \text{sec}]$

ϕ_e = flux density of incident 10 GeV electrons $[\text{cm}^{-2}\ \text{sec}^{-1}]$

$\frac{d\phi_\gamma}{dk}$ = differential flux density of incident photons with energy (k, dk)

t = photon converter thickness (radiation lengths)

$\epsilon_\gamma, \epsilon_e$ = energy flux density carried by photons and electrons respectively $[\text{MeV cm}^{-2}\ \text{sec}^{-1}]$

E_0 = total electron energy [MeV]

$$\epsilon_e = \phi_e E_0 \tag{2}$$

Assume

$$\frac{d\phi_\gamma}{dk} = \frac{t\phi_e}{k} \tag{3}$$

This assumption must satisfy the condition

$$t = \frac{\epsilon_\gamma}{\epsilon_e} \tag{4}$$

and

$$\epsilon_\gamma = \int_0^{E_0} k \frac{d\phi_\gamma}{dk} dk \tag{5}$$

Substitute (3) into (5)

$$\epsilon_\gamma = \int_0^{E_0} \frac{k\phi_e t}{k} dk =$$

$$= t\phi_e E_0 = t\,\epsilon_e$$

$$\therefore \quad t = \frac{\epsilon_\gamma}{\epsilon_e}$$

and Eq. (4) is satisfied.

$$D_e(z) = \phi_e B_e(z) \tag{6}$$

$$D_\gamma(z) = \int_0^{E_0} \frac{d\phi_\gamma}{dk} B_\gamma(z,k)\, dk \tag{7}$$

Substitute (3) into (7)

$$D_\gamma(z) = \phi_e t \int_0^{E_0} \frac{B_\gamma(z,k)}{k} dk \tag{8}$$

Equations (1), (6) and (8) give

$$D(z) = \phi_e t \int_0^{E_0} \frac{B_\gamma(z,k)}{k} dk + \phi_e B_e(z)$$

and

$$t = \frac{\frac{D(z)}{\phi_e} - B_e(z)}{\int_0^{E_0} \frac{B_\gamma(z,k)}{k} dk} \tag{9}$$

Beck has tabulated data for $B_\gamma(z,k)$ for k=0.1, 0.2, 0.5, 1.0, 5.2 and 10.0 GeV. The same quantity has been calculated for k=0.001, 0.01 and 0.05 GeV by using fluence to dose conversion factors for different photon energies, listed in Ref. 19. The integral in Eq. (9) was evaluated graphically from 0.001 GeV to 10 GeV.

$D(z)/\phi_e$ and $B_e(z)$ were taken directly from Fig. 13.

For z = 27.5 cm, Eq. (9) gives t=0.34 radiation lengths.

Conclusion

In order to explain the discrepancy in the dose buildup between this experiment and Beck's Monte Carlo calculation, by the assumption of a photon-contamination, a converter of 0.34 radiation lengths would have had to intercept the electron beam. The experimental arrangement was such that this can be ruled out as a possibility.